NASA/CR-97- 205777

National Aeronautics and Space Administration

Final Report for:

A Preliminary Investigation of Hall Thruster Technology

NAG3-1504

Principal Investigator - Professor Alec D. Gallimore
Department of Aerospace Engineering
The University of Michigan
Ann Arbor, MI 48109-2140
alec.gallimore@umich.edu

9-25-97

Abstract

A three-year, NASA/BMDO-sponsored experimental program to conduct performance and plume plasma property measurements on two Russian Stationary Plasma Thrusters (SPTs) has been completed. The program utilized experimental facilitates at the University of Michigan's Plasmadynamics and Electric Propulsion Laboratory (PEPL). The main features of the proposed effort were as follows: We

- Characterized Hall thruster [and arcjet] performance by measuring ion exhaust velocity with probes at various thruster conditions.
- Used a variety of probe diagnostics in the thruster plume to measure plasma properties and flow properties including T_e and n_e, ion current density and ion energy distribution, and electric fields by mapping plasma potential.
- Used emission spectroscopy to identify species within the plume and to measure electron temperatures.

A key and unique feature of our research was our collaboration with Russian Hall thruster researcher Dr. Sergey A. Khartov, Deputy Dean of International Relations at the Moscow Aviation Institute (MAI). His activities in this program included consulting on and participating in research at PEPL through use of a MAI-built SPT and ion energy probe.

1 Introduction

1.1 Need for High Performance Propulsion

Propulsion systems having high exhaust velocities (U_e >10 km/s) are desirable for a variety of space missions. In order for a propulsive system not to require an inordinate amount of propellant, its exhaust velocity should be of the same order as the characteristic velocity increment (Delta-V) required for a given space mission. Studies have shown that for orbit transfer missions of interest by NASA and the DOD, a characteristic velocity increment of over six kilometers per second may be necessary[1]. Cryogenically fueled chemical rockets which rely on the intrinsic energy available from the chemical reactions of their constituent propellants are inherently limited to exhaust velocities of 5 km/s. Chemical rockets which use "space storable" fuels such as hydrazine are limited to exhaust velocities of 3.5 km/s. Thus, propulsion systems which produce exhaust velocities considerably higher than those obtained with chemical systems would benefit a variety of orbital space missions.

Studies have shown that ideally, an engine which would be used as the primary source of propulsion for orbit transfer missions or for satellite station-keeping should produce an exhaust velocity between 10 and 20 km/s. To achieve this performance, a propulsion system must accelerate its propellant gas without relying on energy addition through chemical reactions. One approach is the application of electrical energy to a gas stream in the form of electrical heating and/or electric and magnetic body forces. This type of propulsion system is commonly known as electric propulsion.

Electric propulsion can be categorized into three groups[2]:

1. In *Electrothermal Propulsion Systems*, a gas is electrically heated, either with resistive elements or through the use of an electric arc, and is subsequently expanding through a supersonic nozzle to produce thrust.
2. *Electromagnetic Propulsion Systems* use electromagnetic body forces to accelerate a highly ionized plasma.
3. *Electrostatic Propulsion Systems* use electrostatic forces to accelerate ions.

In addition to possessing suitable exhaust velocities, an electric propulsion system must be able to convert onboard spacecraft power to the directed kinetic power of the exhaust stream efficiently. Thrust efficiency (cf. Eq. 1), defined as the fraction of thruster power that is converted into directed thrust power, where $\dot{m}$ is the propellant mass flow rate, U_e is the propellant exhaust velocity, and P_t is the total input thruster power, is a measure of how efficiently an electric propulsion system utilizes spacecraft power for thrust.

$$\eta_{th} = \frac{\dot{m} U_e^2}{2 P_t} \tag{1}$$

Electrothermal systems have limited utility for orbit transfer missions because of performance constraints (i.e., low thrust efficiencies) placed on them by excessive frozen flow and electrode losses[3, 4, 5].

Steady-state electromagnetic systems have demonstrated high thrust efficiencies only at power levels that far exceed those generated onboard current spacecraft[6, 7]. However, researchers at NASA are currently evaluating pulsed magnetoplasmadynamic (MPD) thrusters as a means of propelling orbit transfer vehicles with moderate solar power supplies (~10 kW).

Gridded electrostatic engines (e.g. ion engines), which can achieve large exhaust velocities ($U_e > 50$ km/s) at high thrust efficiencies (>0.7), have traditionally demonstrated efficient performance at exhaust velocities above 30 km/s[2, 8, 9], beyond the desired range for orbit transfer missions. Furthermore, ion engines also suffer from acceleration grid erosion due to sputtering from energetic neutrals created by charge-exchange collisions, and from severe power processing mass penalties paid for the large operating voltages (e.g., 2000 V) of these engines.

Therefore, the ideal propulsion system for orbit transfer missions and for satellite station-keeping is one that efficiently accelerates propellant (e.g., through electrostatic means) to modest exhaust velocities while requiring discharge voltages of less than 1000 V. As is shown below, the Hall thruster is a device which fulfills these requirements.

1.2 Background on The Hall Thruster

The Hall thruster is an electrostatic engine that was developed in the 1960s to alleviate the thrust density limitation of ions engines that results from "space-charge" effects within the acceleration volume. These engines were also attractive from the standpoint that since grids are not required to accelerate ions, Hall thrusters do not suffer from the large grid erosion rates of the ion engines. Interest in the Hall thruster waned in the early 1970s because of budgetary cuts and because American researchers were never able to demonstrate that Hall thrusters could operate at thrust efficiencies near those achieved with ion engines[10, 11, 12]. As such, Hall thruster research essentially disappeared in the U.S. between 1972 and 1985. From 1985 to 1990, Ford Aerospace (now Space Systems/Loral), in conjunction with the NASA Lewis Research Center (LeRC), funded a small research effort to determine if Hall thrusters could be used for North-South satellite station-keeping (NSSK). This program proved to be unsuccessful and was abandoned.

Throughout this period however, Hall thruster research flourished in the Soviet Union. Hall thrusters were first tested in space in 1971 with immediate success[13, 14]. Since then, over seventy Hall thrusters are claimed to have been used onboard Soviet spacecraft (mostly as plasma contactors). Recently, because of claims made by Russian researchers[1] of high thrust efficiency (~40-75%) at specific impulses that are ideal for missions in earth orbit (1600 seconds), there has been a great deal of interest in using Russian-made Hall thrusters on American spacecraft. Clearly, such a device with performance far superior to that of arcjets, currently the most advance propulsion system proposed for American spacecraft, would not only serve as an excellent thruster for NSSK, but potentially could be scaled in power to propel orbit transfer vehicles.

1.3 The Hall Thruster

There are two types of Hall thrusters that have been studied at great lengths, the end-Hall thruster and the closed-drift thruster. Both engines, in principle, are capable of producing specific impulses in excess of 1500 seconds with xenon at a thrust efficiency ~50%.

---

[1] Most of these claims have been substantiated by a team of American researchers who traveled to Russia and evaluated the performance of a 1.35 kW Hall thruster.

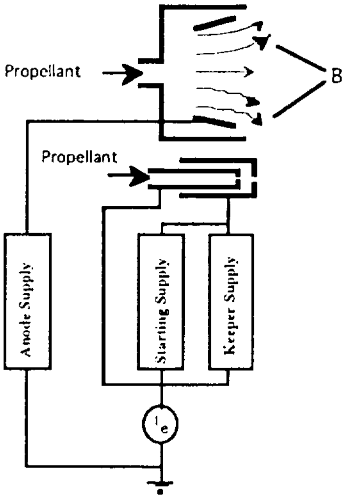

Figure 1: Schematic diagram of an end-Hall thruster.

The end-Hall thruster is a gridless electrostatic device in which propellant is first ionized in the discharge chamber and then accelerated by an axial electric field produced by the interaction of the discharge current with an applied diverging axial magnetic field (cf. Figure 1). This magnetic field is supplied by either permanent magnets or a solenoid. As is shown in Figure 1, multiple power supplies are needed to run this type of thruster, the most demanding of which is needed to supply the discharge current. These thrusters are typically between ten and twenty centimeters in diameter and operate at power levels of a few kilowatts or less. The applied magnetic field strength is usually selected so that the electron conductivity parallel to the magnetic field lines is much greater than the transverse electron conductivity;

$$\sigma_{\|} \gg \sigma_{\perp}. \tag{2}$$

This typically corresponds to an applied field strength on the order of 0.1 T (1000 Gauss).

In accordance to Equation 2, one would expect equipotential lines to be parallel with magnetic field lines. However, numerous experiments have found that substantial voltage gradients exist parallel with the magnetic field, in approximate agreement with the following expression [15]

$$\Delta V_p = \frac{kT_e}{e} \ln(\frac{B}{B_o}) \tag{3}$$

where k is the Boltzmann constant, T_e is the electron temperature, e is the elementary electric charge, and B/B_o reflects the variation in magnetic field strength over the extent at which the change in voltage (ΔV_p) is calculated. It is this voltage drop, calculated over the entire extent of the discharge chamber, that is responsible for the acceleration of the ionized propellant.

The other variant of Hall thruster, the type that was frequently used in the former Soviet Union over the past twenty years, is a variant of the closed-drift Hall accelerator (cf. Figure 2) called the Stationary Plasma Thruster (SPT). The SPT is a coaxial device in which a magnetic field that is produced by an electromagnet is channeled between an inner ferromagnetic core (pole piece) and outer ferromagnetic ring, resulting in an essentially radial magnetic field. An axial electric field is provided by applying a voltage between the anode and the downstream cathode. Insulation is used to prevent the plasma from shorting out the discharge through the magnet pole pieces. The perpendicular electric and magnetic fields establish an azimuthal electron Hall current.

In its basic form, acceleration in the SPT thruster arises from the force generated by the cross product of the radial magnetic field with the azimuthal Hall current formed from the $\vec{E}$x$\vec{B}$ drifts of the electrons. The magnetic field strength is generally chosen so that the length of the accelerating channel is much larger than the electron Larmor radius, but is much smaller than the ion Larmor radius, so that in principle, the magnetic field suppresses the axial mobility of the electrons while exerting essentially no effect on the ion dynamics. As a result, the plasma can support an axial electric field with a potential difference close to the applied voltage between the electrodes. This electric field provides the mechanism for ion acceleration.

Although they vary in size and input power (e.g. 7 cm in diameter at 660 W and 20 cm in diameter at 6 kW), SPT's that are currently being considered for satellite NSSK roles have input power levels between 0.5 and 3 kW and propellant (xenon) flow rates up to 10 mg/s. These devices typically operate at a discharge voltage of approximately 300 V at a few amperes of current. Up to 80% of this discharge voltage is effectively utilized in the acceleration of the bulk of the propellant. This accounts for the fact that approximately 50% of the thruster input power is converted into directed kinetic power. Although Hall thrusters have characteristics that make them ideal for stationkeeping and orbit transfer applications, these devices have specific problems which make the integration of them with spacecraft an interesting challenge. This problem is the primary motivation for the proposed work.

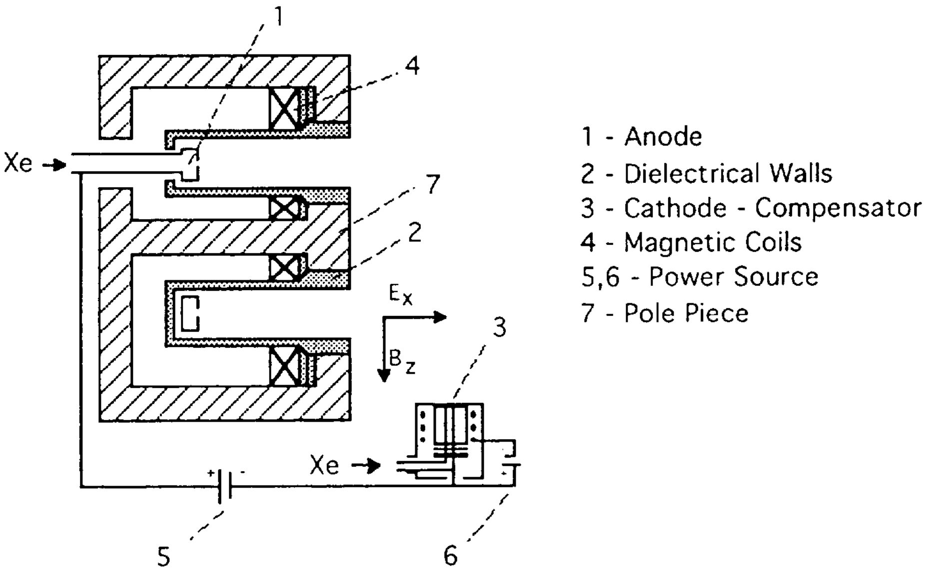

Figure 2: Schematic diagram of a Russian Stationary Plasma Thruster.

1.4 Motivation for Research Program

Some key problems that plague these engines are described in the following sections. The section describes problems that are germane to the efficient operation of these thrusters.

1.4.1 Thruster Specific Engineering Issues

One of the reasons that the Hall thruster was abandoned in the United States was that the thrust efficiencies of these engines never approached those obtained by gridded electrostatic thrusters. The three major factors that led to the deficient performance of the Hall thrusters were that: (i) a small fraction of the ionized propellant was accelerated by the electrostatic field; (ii) the electron diffusion rate through the magnetic field was too large; and (iii) a large fraction of the exhaust kinetic energy of the ions was lost due to ion impact with the discharge channel walls.

To quantify these deficiencies, use is made of the following terms[16]. The *propellant utilization*,

$$\eta_u = \frac{m_i J_b}{e\dot{m}} \tag{4}$$

where m_i is the ion mass, J_b is the ion beam current, and $\dot{m}$ is the propellant mass flow rate, is a measure of how much of the propellant is ionized and utilized as beam current. The *acceleration efficiency*,

$$\eta_a = \frac{J_b}{J_a} \tag{5}$$

where J_a is the total discharge current, describes the fraction of thruster current that is composed of accelerated ions. Assuming that only singly-charged ions are produced, the thrust can be written as

$$T = J_b \sqrt{2m_i V_m / e} \tag{6}$$

where V_m is the average ion beam energy calculated by suitably averaging the ion beam energy distribution. Neglecting power needed for the magnet(s) or for heating the hollow cathode or cathode filaments, the thrust efficiency of the Hall thruster can be written as

$$\eta_{th} = \frac{T^2}{2\dot{m} J_a V_a} \tag{7}$$

where V_a is the total voltage drop through the discharge. Defining the fraction of the discharge voltage that is utilized in propellant acceleration (*beam energy efficiency*) by the following equation

$$\eta_e = \frac{V_m}{V_a}, \tag{8}$$

and substituting Equations 4, 5, 6, and 8 into Equation 7 yields

$$\eta_{th} = \eta_u \eta_a \eta_e \tag{9}$$

Therefore as Equation 9 suggests, thrust efficiency suffers when a small fraction of the propellant is ionized, a large portion of the discharge current is carried by the electrons (due to anomalous cross-field diffusion for example), or when a small fraction of the discharge energy is used to accelerate the exhaust ions.

Researchers in the Soviet Union were able to combat many of these problems by manipulating the applied magnetic field profile of these engines. By applying a highly convex magnetic field that monotonically increases axially from the anode to the cathode, the Soviets were able to substantially decrease the rate of cross field diffusion of electrons due to plasma instabilities while reducing the number of accelerated ions that collide with the insulator walls[14]. In addition, by using xenon instead of argon, the propellant most American Hall thruster researchers used, the Soviet thrusters were able to operate with a much higher fraction of propellant utilization than their American counterparts. As a result of these changes, Soviet Hall thrusters are able to operate at thrust efficiencies twice as high as those obtained in the United States. It is this technical expertise in the Hall thruster physics, which exists only in the former Soviet Union, that we applied in our research.

Although the performance of the Hall thruster is promising as is evident from the recent set of measurements made at the NASA LeRC [17], there are still a great deal of questions that surround the operation of these devices. For example, in the tests reported in Ref. [17], a SPT that the Russians are trying to commercialize for satellite station-keeping (SPT-100) was found to the be very sensitive to background chamber pressure and cathode flow rate. By metering xenon into the chamber through a chamber side port, these researchers were able to vary chamber pressure by over an order of magnitude. Specifically, they found that for many operating conditions, thruster performance improved with increasing chamber pressure up to a point. Beyond this point the thruster would become unstable exhibiting large current and plume oscillations the latter of which were visible to the naked eye. In fact, the thruster periodically entered times of oscillatory operation which inexplicable would follow and preface periods of quiescent operation [17]. As the tests progressed in time, the envelope of stable thruster operation collapsed towards the so-called "design operating point." Other recent experimental programs that conducted SPT performance and life-time testing and plume plasma property measurements also reported equally odd thruster behavior [18, 19]. This clearly illustrates that much of the underlying physics of these devices are not well understood.

2 Summary of Results

Activities during the initial portion of the funding period centered around facilities modification and development diagnostics needed for plume characterization. Experiments with Hall thrusters soon followed. The diagnostics that were developed over this initial period included a thrust stand, Langmuir probe, the impact pressure probe, emission spectroscopy, the retarding potential analyzer, and the emissive probe. A microwave interferometer was also developed and used at PEPL under a separate activity. Because a closed drift thruster was not available for most of this period, most of these measurements were made with an end-Hall thruster and an arcjet, both of which were supplied by NASA LeRC. It was not until September 1994 that experiments with a stationary-plasma thruster, supplied by the Moscow Aviation Institute, commenced (see below).

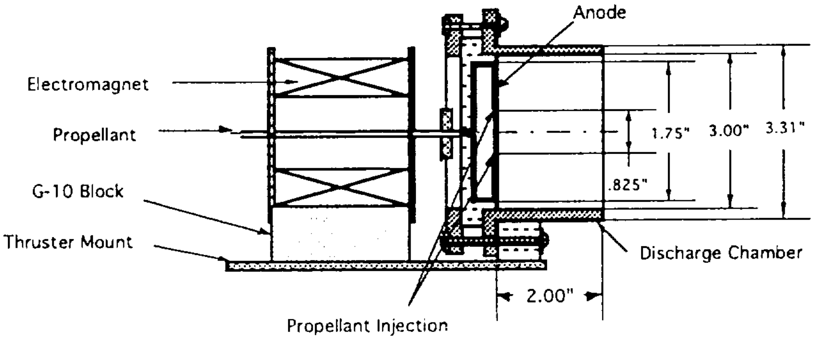

Figure 3: Schematic diagram of the 500 W end-Hall thruster.

2.1 Results with the end-Hall Thruster

Figure 3 shows a cross sectional view of the 0.5 kW-class end-Hall that was supplied by the NASA LeRC for this study. The engine is composed primarily of four components: 1) the cathode (not shown on figure); 2) the anode; 3) the discharge chamber; and 4) the magnet (solenoid).

The cathode used for this study is the standard hollow cathode used in xenon ion thrusters at NASA LeRC. The cathode consists of a 0.25-inch-diam. by 4-inch-long molybdenum-rhenium tube. A thoriated-tungsten end-plate with a 60-mil-diam. orifice is electron-beam welded to one end. The other end of the cathode contains fittings for propellant delivery. The cathode insert is a sintered tungsten cylinder impregnated with $4BaO\text{-}CaO\text{-}Al_2O_3$. The cathode is situated at the "12-o'clock" position above the discharge chamber, pointing approximately 45 degrees toward the center with its orifice some 0.75 inches downstream of the discharge chamber exit (2.75 in downstream of the anode).

The anode used for the thruster serves as the primary propellant delivery system as well. The anode is a 1.75-inch-diam molybdenum disc recessed within the 2-inch-long by 3-inch-diam. (i.d.) molybdenum discharge chamber (cf. Figure 3). The anode contains twelve propellant injection holes, each located 0.825 inches radially from the anode centerline. The discharge chamber rests on a Macor block that is bolted to an aluminum thruster mount. The discharge chamber is insulated from the anode with boron-nitride.

The magnetic field is supplied by a solenoid located 0.25 inches behind the discharge chamber. The solenoid rests on a G-10 block that is bolted to the aluminum mount and consists of approximately 60 turns of #6 gage solid copper wire wrapped around a soft-iron spool. At a solenoid current of 10 A, the maximum radial magnetic field strength measured in the discharge chamber was approximately 12 G. The the maximum magnitude of the magnetic field within the chamber is estimated to be 25 G. Thus, modifications were made to the original design to increase field strength. These included surrounding the discharge chamber with a soft-iron ring, and using iron bars to more efficiently conduct the magnetic field from the solenoid to the ring. This modification increased the maximum field strength within the chamber to 75 G (at 10 A). Although this value is still too low to provide an effective means of ion acceleration, it is of sufficient strength to magnetize the electrons. Details of the design modifications are given below.

Figure 4 shows a schematic of the power supply circuit used to operate the thruster. Four power supplies were used for the thruster; one each for the discharge, the cathode heater, the magnet, and the ignitor/keeper electrode. Hall thruster main discharge power is provided by a 10 kW Sorenson DCR 600-16T power supply that is capable of providing 16 Amps of current at 600 V. This power supply is connected in series with the thruster through a variable ballast resistor. Magnet and cathode heater power are provided by Kikisui voltage and current regulated DC power supplies. The ignitor supply was custom built for this application and is based on a design used at NASA LeRC to ignite ion thrusters. The ignitor can provide 2000 V DC at a maximum current of 200 mA. Although the negative lead of the ignitor is always connected to the cathode, the positive lead can be connected either to the anode or the ignitor electrode (cf. Figure 4). A series of high current (12 A) 1000 V blocking diodes is placed along the discharge power supply line to protect the Sorenson from high voltage when the ignitor is used at the anode. However, since the thruster was found to ignite more readily when the ignitor electrode is used, only the ignitor electrode was used in starting the Hall thruster. Usually an ignitor voltage of 300-500 V was required to ignite the engine.

Hall thrusters typically operate with radial magnetic field strengths between 100 and 500 G and discharge voltages of a few hundred volts at a few amperes of discharge current. Since the maximum field strength in the discharge chamber of the original thruster was measured at less than 100 G for the maximum current the solenoid can tolerate (30 A), the likelihood of achieving acceptable performance with this device is nil. This was latter verified with initial end-Hall thruster runs.

Initial attempts to start the thruster failed. It was learned that the thruster was operated only briefly at NASA LeRC prior to being shipped to PEPL and that the cathode of the engine may have been damaged during the LeRC test and by prolonged exposure to the atmosphere during its year-long storage at PEPL. After activating the

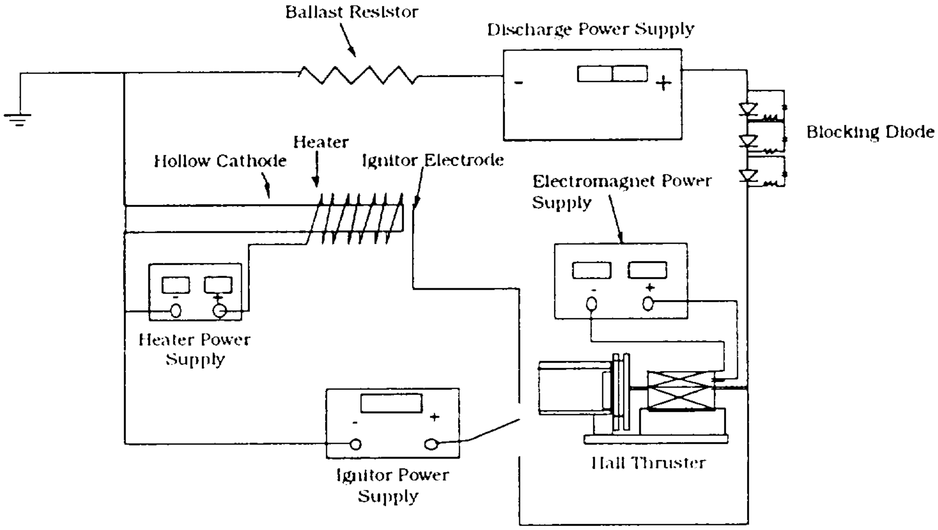

Figure 4: Power supply circuit of the end-Hall thruster.

cathode with hydrogen several times to remove excess moisture, the thruster started.

At a discharge current of 5 A, and a total argon mass flow rate of 2.4 mg/s with a 25% cathode flow fraction (i.e., 0.6 mg through the cathode and 1.8 mg/s through the anode), the discharge voltage remained below 55 volts. Increasing the solenoid current from 1 to 10 A had little effect on the discharge voltage. Considering the losses incurred from ionization alone (tens of eV per ion), this voltage is far too low to yield acceptable thruster performance. Thus, modifications were made to the thruster to increase the local field strength.

A schematic of the modified device is shown in Figure 5. The solenoid was moved slightly closer to the anode, to within ~0.20 inches of the discharge chamber (the closest possible with this design). Highly permeable pieces of soft-iron were machined into pole pieces to conduct the magnetic field to the discharge chamber. An iron tube was placed between the anode and the electromagnet, and an iron ring was slipped around the discharge chamber such that the rear portion of the ring is aligned with the anode surface. To complete the magnetic circuit, two iron loops were fastened to the ring pole piece and the rear pole of the electromagnet. This design places iron along most of

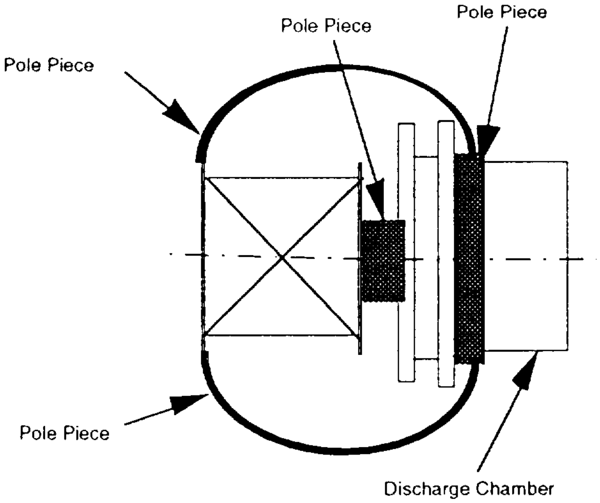

Figure 5: Schematic of the modified end-Hall thruster.

the path that the most intense portion of the solenoid magnetic field would naturally propagate through. The portion of the circuit that is open corresponds to the anode region of the discharge.

Figure 6 shows a comparison of the radial magnetic field profile of the original thruster compared to that after the modifications were made. Small radial and axial Hall probes were used to map the magnetic field throughout the discharge chamber. The position of the Hall element with respect to the sensor tip dictated how close to a solid boundary measurements could be made. In general, the modifications resulted in a three-fold increase in radial magnetic field strength for a given solenoid current. With an operating current of 10 A, the magnetic field of the original design was observed to fall off to negligible values within 0.25 inches of the anode, whereas more reasonable values, however small, were measured after the modifications were made.

The modified thruster maintained stable operation at 5 A, a total argon mass flow rate of 1.7 mg/s (20% cathode flow fraction) for approximately 45 minutes before failing. The modifications increased the discharge voltage at this condition from 45 V to 90 V. Tank pressure was approximately 0.003 Pa (3×10^{-5} Torr) during this test. The cause of the failure was never determined but is thought to be a short between the ignitor

a) Original

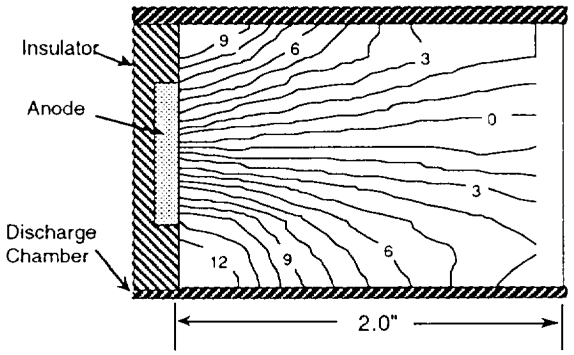

b) Modified

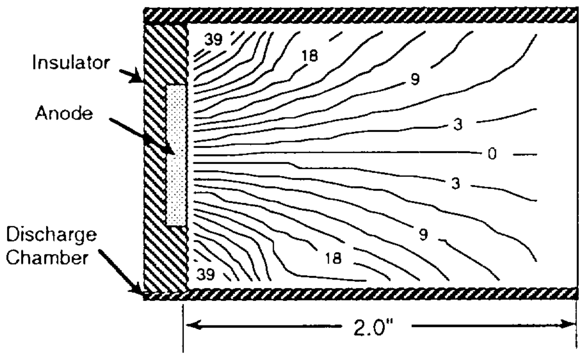

Figure 6: Solenoid radial magnetic field profile (all values are in Gauss).

electrode and the cathode. Only thrust, Langmuir probe, and emission spectroscopy data were collected during this run.

A radiation-cooled version of the NASA LeRC thrust stand was used for all performance measurements in conjunction MKS mass flow meters/controllers. Attempts at making thrust measurements with end-Hall thruster, however, were largely unsuccessful. A specific impulse of 190 sec was measure when the solenoid coil was set to ~2 A. Although "modest" in comparison to the SPT-100, the measured specific impulse is high enough to suggest that the argon heavy particle temperature is probably on the order of 1 eV, since most of this thrust is most likely due to the random thermal expansion of the plasma from the thruster chamber. Attempts at measuring thrust with higher solenoid currents failed (e.g., negative thrusts were measured), most likely because of insufficient shielding and/or thermal drifts.

A cylindrical single Langmuir probe, with a 9-mil-diam. by 0.75-inch-long tungsten wire collector electrode, was used to measure n_e and T_e in the near-field thruster plume. The electrode of the probe is attached to the center conductor of a triaxial boom that is constructed of titanium with Teflon insulation. The boom is approximately 0.166 inches in diameter and 7 inches long.

The collector electrode of the probe was biased with respect to the chamber wall with a Kepco model BOP 100-2M programmable bi-polar power supply. A function generator was used to provide the 12.7 Hz triangular source waveform that was amplified to ±50 V by the bi-polar supply.

Current through the small probe was measured with a 100 Ohm shunt. Probe voltages measured with respect to tank ground were collected with voltage probes and operation amplifiers. Amplifier output signals were collected both by the data acquisition system (LabView) for storage and later processing, and by a Tektronix 500 MHz digital oscilloscope for real-time processing. The data acquisition system stored 50 pairs of probe voltage-current data points per voltage ramp.

All near-field measurements were made with the tip of the Langmuir probe placed 1.2 inches downstream of the discharge chamber exit. For these measurements, the probe was quickly moved to the collection site, kept there long enough to collect ten ramps of data (~1 sec), and rapidly move out of the plume to allow for probe cooling. This approach also served as an effective means of cleaning the probe and could be used to probe within the discharge chamber.

Figure 7 shows electron number density versus radius taken 1.2 inches from the thruster exit. The thruster was operating at a current of 5 A, a total mass flow rate of 1.7 mg/s (20% through the cathode), and a solenoid current of 30 A. Tank pressure was measured at 3.7×10^{-5} Torr during these measurements. Because of excessive signal noise on the Langmuir probe traces, realistic electron temperatures could not

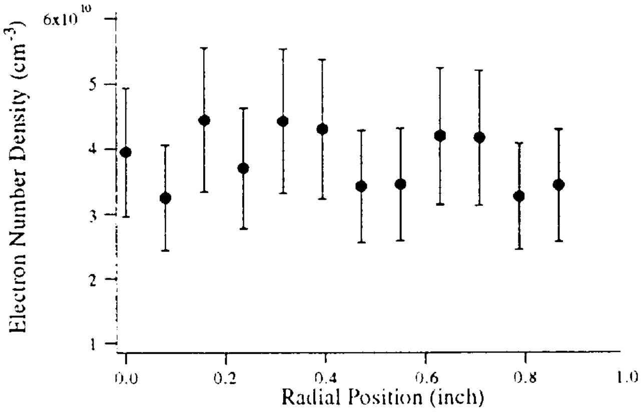

Figure 7: Electron number density profile 1.2 inches from thruster exit plane.

measured. Therefore, an electron temperature of 2 eV was used for determining the electron number density from the ion saturation current. The value of 2 eV is based spectroscopic data described below.

Over a 1 inch region, the electron number density remains relatively flat at a density of ~4 x 10^{10} cm^{-3}. The scatter in the data is a reflection of the periodic changes in thruster operating conditions that were observed.

Thruster current was maintained by operating the Sorenson power supply in constant current mode. Thus, discharge voltage is automatically adjusted to maintain the set current. Over the course of a few minutes however, the discharge voltage would vary by as much as 20 volts (i.e., 85±20 V) before returning to its original value. The reason for this low frequency oscillation has not been determined, however, similar phenomena have been seen in other Hall thruster experiments[17].

Emission spectroscopy was used to estimate the electron temperature near the exit plane of the thruster. An achromatic lens was used to collect light 0.5 inches downstream of the thruster exit plane along the centerline. The light collected by the lens was focused onto a silica optical fiber which carried the light out of the vacuum chamber to the collection optics at the spectrometer. A Spex 500M spectrometer, fitted with an 1800 grooves/mm holographic grating blazed at 500 nm, was used to analyze the light collected at the entrance slit. Both the entrance slit and the exit slit were set at 100 microns to maximize the amount of light collected.

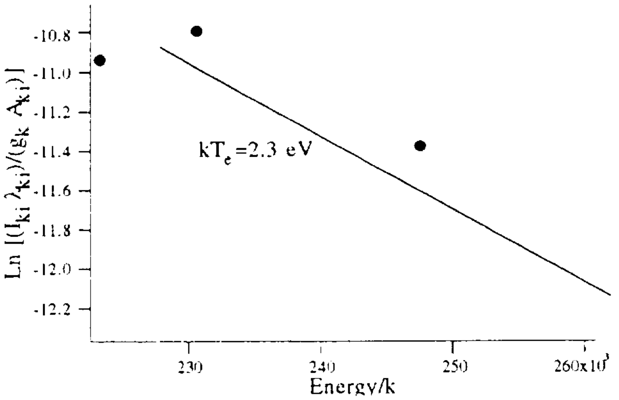

Figure 8: Boltzmann plot of excited states.

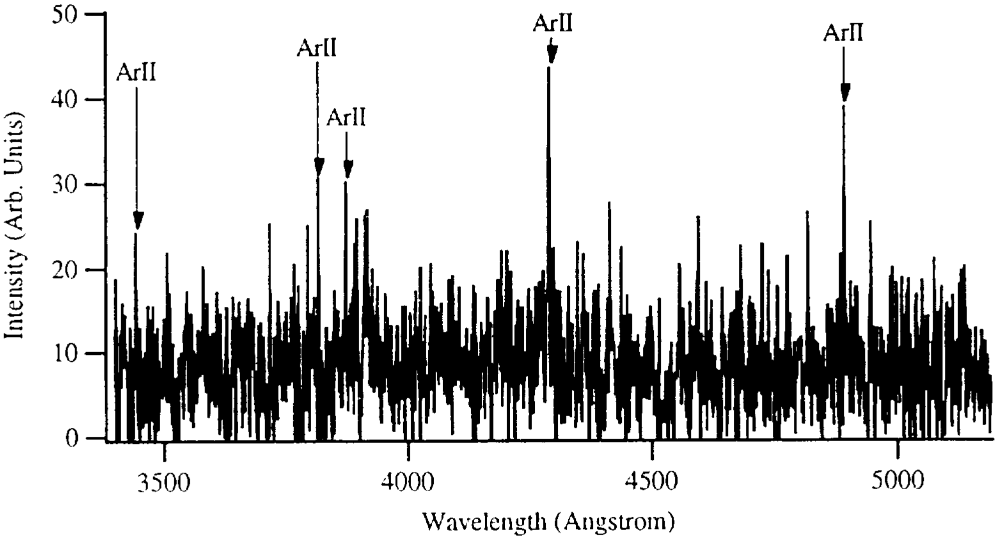

Figure 9: Measured emission spectra.

Spectra were acquired in the 340-520 nm range in an attempt to obtain information from those excited states with energies near the ionization boundary. Such states are spaced closely together and are good candidates to be in equilibrium with the electrons. For these measurements, the thruster was operated at a current of 5 A, a total mass flow rate of 1.7 mg/s (20% through the cathode), and a solenoid current of 30 A.

The portion of the argon spectrum analyzed contained both singly ionized argon lines and neutral lines, however, the strongest signals obtained in this region of spectra came from ArII (singly ionized) lines. To minimize errors associated with intensity measurements, only lines associated with singly ionized argon were used in the Boltzmann plot for calculating T_e. Although the lines acquired were on the order of 5 eV below the ionization potential of singly ionized argon, the lines were still somewhat closely spaced together in energy.

Four lines - 381 nm, 428 nm, 440 nm, and 455 nm - were used for the Boltzmann plot of Figure 8. The selected points from the spectra match the line-fit rather well. An electron temperature of is 2.3 eV is calculated from the slope. Because the intensity contributions come from a chord along the plume cross section, this temperature should be thought of as a plume-integrated average electron temperature across the centerline at this axial location.

The measured emission spectra from the engine are shown in Figure 9. Labeled on the graph are prominent ArII lines. No strong lines for neutral or doubly ionized argon were observed.

2.2 Results with the Arcjet

Because the arcjet was the first operational engine at PEPL, it was used as a vehicle for developing and testing diagnostics. A standard lab-model 1 kW arcjet and PPU (both supplied by NASA LeRC) were used for this work. The engine features a 2%-thoriated tungsten cathode and a nozzle (also of 2%-thoriated tungsten) that serves as the anode. The arcjet has a 0.51-mm-diam. by 0.25-mm-long constrictor, a 30 degree half-angle converging nozzle section upstream of the constrictor, and a 20 degree half-angle diverging section. The exit diameter of the nozzle is 9.52 mm, giving the expansion section an area ratio of 350. The electrode gap spacing is 0.51 mm. The outer housing of the device is constructed of titaniated zirconiated molybdenum (TZM).

Arcjet power is provided by a 1800 Watt Sorenson power supply that is conditioned by a NASA LeRC Power Processing Unit (PPU). The PPU nominally operates at output voltages between 100 and 120 Volts and at currents between 6 and 12 A with ±1.5 A ripple.

For plume measurements the thruster was nominally operated at a current of 10 A on pure hydrogen at a mass flow rate of 15 mg/s. Thruster voltage was approximately

Propellant	I_{sp} (sec)	Efficiency (%)
N_2H_4 (47 mg/s)	426	36
NH_3 (38 mg/s)	411	30
H_2 (15 mg/s)	700	32

Table 1: Summary of arcjet performance at 10 A.

110 V at this condition. However, performance measurements were made with the thruster operating on simulated hydrazine and ammonia as well. Tank pressure was maintained to 0.04 Pa (3 x 10^{-4} Torr) during all plume measurements.

The arcjet was allowed to run for a 20 minute warm-up period after ignition before measurements were made. This time was determined to be the duration needed for the arcjet to reach thermal equilibrium on the basis of the discharge voltage. Performance measurements were made with simulated N_2H_4 at 47 mg/s, simulated NH_3 at 38 mg/s, and pure H_2 at 15 mg/s.

Figure 10 shows arcjet performance data for simulated hydrazine at 47 mg/s and for currents between 6 and 12 A; the entire range of the PPU. Thrust efficiency is calculated with the following equation:

$$\eta_{th} = \frac{{I_{sp}}^2}{(\frac{2}{g^2})(\frac{P_a}{\dot{m}})}. \tag{10}$$

This definition of thrust efficiency does not take into account cold-gas thruster performance, nor does it include corrections to I_{sp} for background pressure effects.

As the figure shows, thrust efficiency ranges between 30 and 40%, and specific impulse is between 350 and 450 sec. Since the thrust and I_{sp} measurements are expected to be accurate to within a few percent at low power levels (i.e., current below 10 A), the smaller error bars on the figures represent the spread in raw data, typically 5-7%. For currents above 10 A, thrust was measured to *decrease* with increasing power. This is obviously a result of excessive thermal drifts of the thrust stand. Attempts at taking this drift into account after the arcjet was turned off were not successful since thermocouples attached to the stainless-steel shell showed that once the arcjet is turned off, the thrust stand quickly cools off prior to the post-run calibration.

Although not shown on the figure, performance measurements with NH_3 and H_2 at 10 A and the mass flow rates noted above were also made. Typical values are presented in Table 1.

Near-field Langmuir probe measurements were made with probe described above in the end-Hall thruster summary. A function generator was used to provide the 12.7 Hz

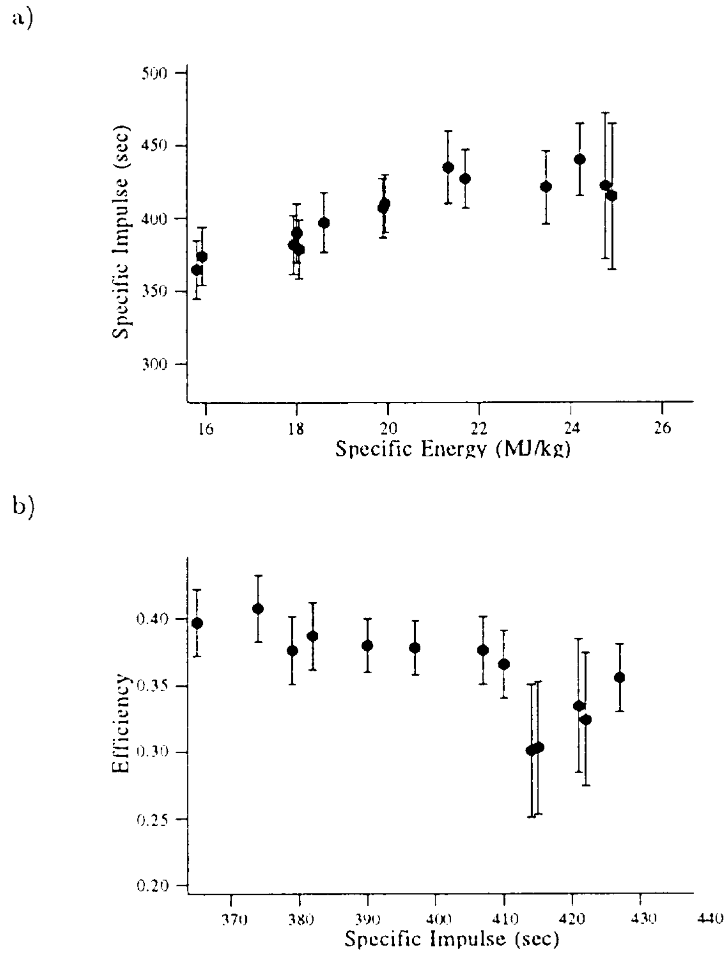

Figure 10: Arcjet performance data for simulated hydrazine ($\dot{m}$=47 mg/s).

triangular source waveform that was amplified to ±10 V by the bi-polar supply.

All near-field measurements were made with the tip of the Langmuir probe placed 20 mm downstream of the nozzle exit. To collect data this close to the exit, the probe was quickly moved to the collection site at the appropriate angle (see next paragraph), kept there long enough to collect ten ramps of data (~1 sec), and rapidly move out of the plume to allow for probe cooling. This approach also served as an effective means of cleaning the probe since the probe electrode was observed to glow as it was removed from the plume.

Since in the near-field region of the plume $r_p/\lambda_D \geq 10$ and $\lambda_i/r_p > 100$, the standard collisionless thin sheath Bohm ion saturation current model was used to interpret Langmuir probe data. To account for ion current collection due to convection from the flowing plasma, the probe angle was varied between 0 and 10 degrees with respect to the plume axis of symmetry. 10 degrees was determined to be the maximum angle possible for the boom of the probe not to perturb the flow significantly.

Figure 11 shows radial electron temperature and number density profiles. As the figure shows, electron number density measurements are quite sensitive to probe angle. The peak value of n_e (slightly offset from the axis) at 10 degrees is more than twice that with the probe aligned with the thruster axis. However, the n_e data for the three probe orientations converge with increasing radius, and identical values are predicted 18 mm from the centerline. LIF measurements have shown the axial velocity of hydrogen arcjets to decrease rapidly with radius[20]. Thus, the fact that probe angle has little influence on number density measurements at this location may be an indication that the local flow velocity is close to the heavy particle thermal speed, and so convective ion collection at the probe becomes indistinguishable from random flux collection.

Higher than expected electron temperatures were measured with the Langmuir probe. Electron temperature is seen to decrease with increasing probe angle but to remain relatively constant with radius. This last trend has been observed in higher powered hydrogen arcjets (10 kW) via emission spectroscopy[21]. Only the 10 degree probe data show expected values of T_e. The reason for this probe angle dependence is not known at this time.

In order to measure electron temperatures and densities one meter from the arcjet exit plane and beyond (the far-field), where λ_D is on the order of 0.1 mm[4], a 0.42-cm-diam. by 5.1-cm-long rhenium cylindrical Langmuir probe was used. The collector electrode was formed by vapor-depositing rhenium on a molybdenum mandrill.

In the far-field, λ_e and λ_i are expected to be an order of magnitude larger than the diameter of the large probe and at least two orders of magnitude larger than the sheath. Furthermore, since r_p/λ_D will be approximately 20 or more for the large probe, a thin sheath saturation current model was used to analyze data from this probe. The probe

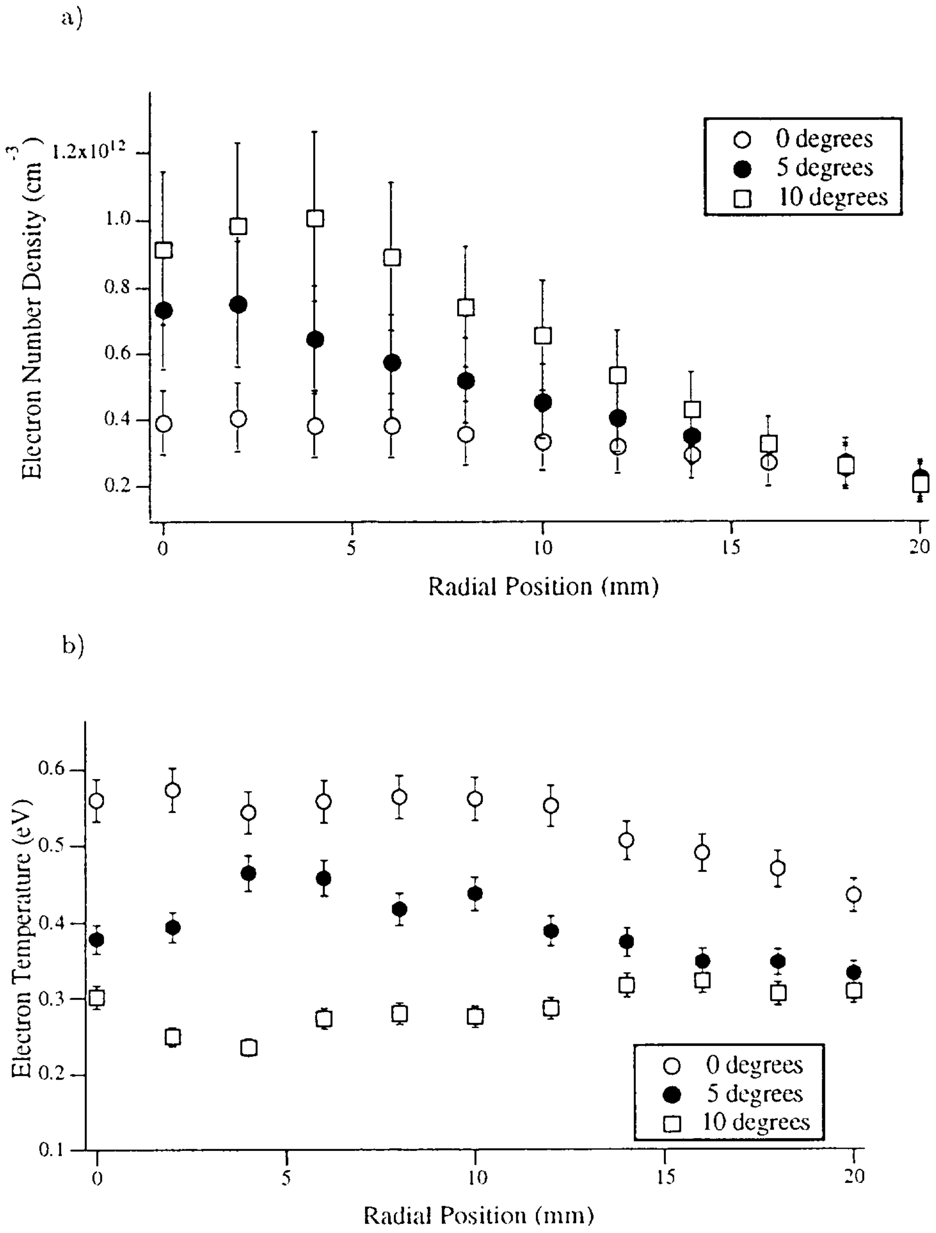

Figure 11: Electron number density and temperature profiles.

was cleaned chemically (with Acetone) prior to each test.

Figure 12 shows profiles of electron temperature and number density as measured with the large probe using the thin sheath model. The probe angle was rotated to 0, 5, 10, 20, and 30 degrees with respect to the thruster axis at each location. The table position was adjusted automatically at each angle to ensure that the collector electrode of the probe was in the appropriate axial and radial positions. The probe was moved continuously at a radial speed of 1.2 cm/s. Thus, 50 pairs of probe voltage-current data points were collected per millimeter of radial travel (voltage ramp). A Hewlett-Packard workstation running MATLAB was used to process the tens of thousands of data points to obtain electron temperatures and number densities. Only data collected at angles at which the axis of the probe is aligned with the local flow (i.e., minimum ion saturation current) are reported.

As the figure shows, the peak number density drops from 5×10^9 to less than 2×10^9 cm^{-3} over a half-meter increase in axial position. At 30 cm from the exit, the number density at the edge of the measurement region is nearly an order of magnitude smaller than the peak value. At the 88 cm position, the radial electron number density profile is flat, suggesting that the exhaust rapidly assumes a uniform spherical expansion pattern. The variation in electron temperature, however, is not nearly so dramatic and is approximately 0.1 eV at both axial locations. The increased scatter and higher indicated temperature at the fringe of the measurement region may be due to probe misalignment with the flow.

All spectra were taken with the arcjet operating at 10 A at a mass flow rate of 15 mg/s of pure hydrogen with spectrometer described above. Data were taken by translating the fiber optics/lens assembly via a stepper motor-driven linear stage in 1 millimeter increments perpendicular to the plume axis 12 mm downstream of the exit plane and 15 cm to the side of the arcjet centerline. The spectrometer entrance slit was set at 100 microns to maximize the amount of light collected by the spectrometer while the exit slit was set at 500 microns to ensure capture of Stark broadened hydrogen lines. A chopper and lock-in amplifier was also used to maximize signal fidelity. The emissivity coefficient for each measured transition was then calculated from intensity profiles along various chords of the plume via Abel inversion. With the emissivity coefficient, Boltzmann plots were then made to determine the electron temperature as a function of radius.

Figure 13 a) shows examples of Boltzmann plots made at three radial locations, 12 mm downstream of the exit plane. The 434 nm, 410 nm, and the 397 nm Balmer lines were used for this plot. The linearity of this plot suggests that the upper states used in the Boltzmann plot are in local thermal equilibrium with the electrons and can be used to measure electron temperature.

a)

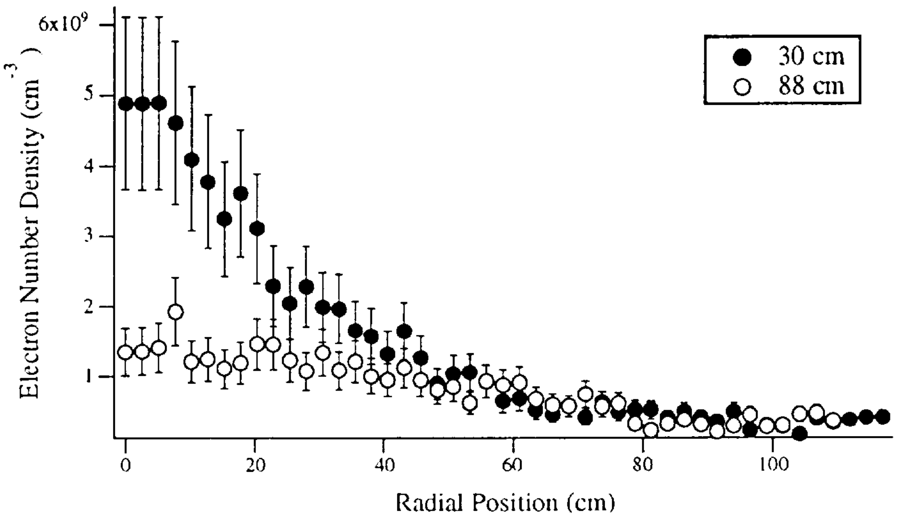

b)

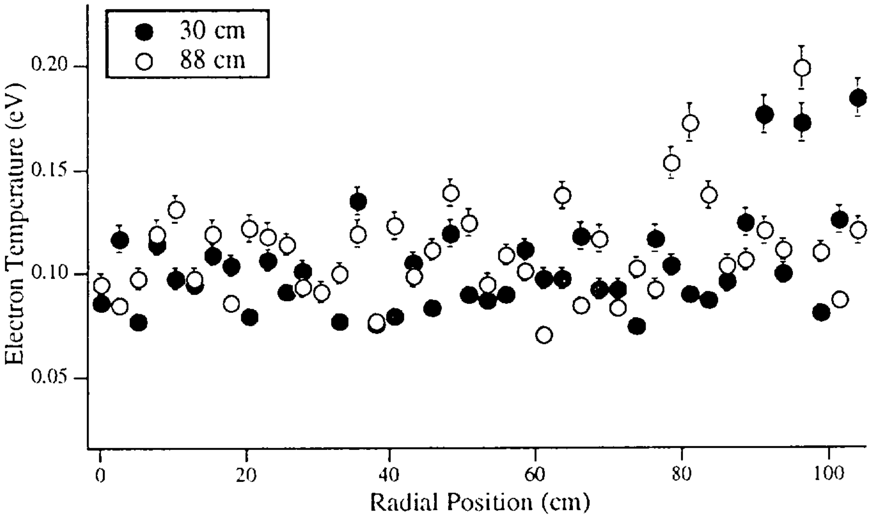

Figure 12: Electron number density and temperature profiles.

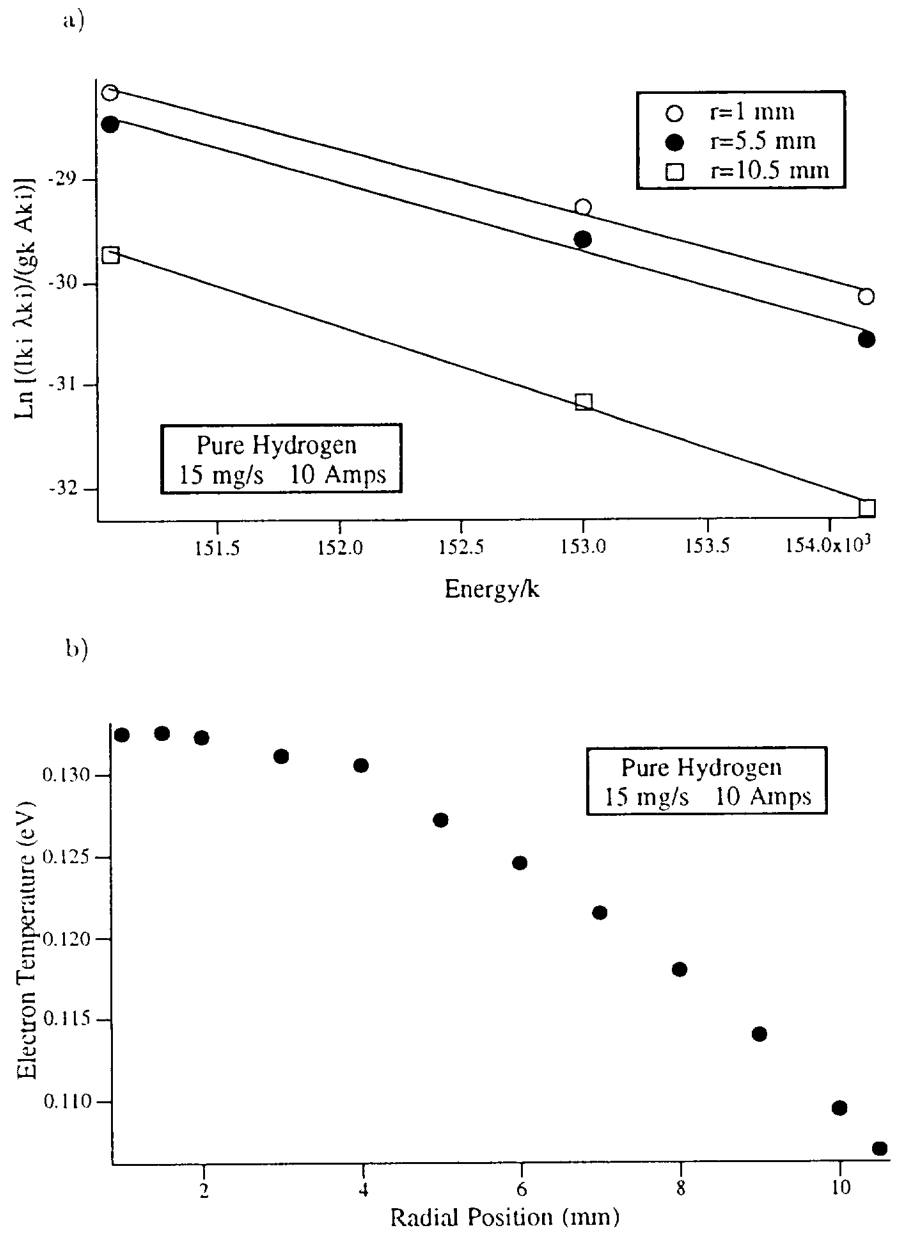

Figure 13: Boltzmann plot of excited states, and corresponding Electron temperature vs. radius with H_2 propellant.

Figure 13 b) plots electron temperature, determined from the Boltzmann plot, as a function of radial position. As the figure shows, the electron temperature drops off rapidly with radius. The peak electron temperature of ~0.13 eV is found near the center of the plume. At 10.5 mm from the plume center, the electron temperature drops to less than 0.11 eV. Initially, four hydrogen Balmer lines were used in this study for making Boltzmann plots; the 486 nm, 434 nm, 410 nm, and the 397 nm lines. It was observed, however, that the electron temperatures predicted with these Boltzmann plots increased with radius, a trend which is counterintuitive. This behavior suggests that the low lying states on the plot may not be in equilibrium with the electron energy distribution.

The 486 nm state lies 0.31 eV below the nearest upper exited state in the Balmer series. As a consequence of the wide (relative to T_e) energy spacing between this state and its nearest upper excited state, it is improbable that the electrons are in equilibrium with it. Additionally, the intensity of this state decreases with radius as the true electron temperature and density decreases, and as the lower lying excited states in general fall further out of equilibrium. This results in a flattening of the slope of the Boltzmann line at large radii, resulting in artificially high T_e. This low lying state was thus removed to make Figure 13 a), and the data were refitted to predict the electron temperature profile shown in Figure 13 b). The electron temperatures calculated from the the corrected Boltzmann plot are consistent with the energy spacing between these upper states. This finding suggests that the upper states used in Figure 13 a) are in local thermal equilibrium with the electrons and can be used to measure electron temperature.

Of concern is the disagreement between Langmuir probe and spectroscopy T_e data. The source of this discrepancy is unknown at this time, however, future experiments will be performed to resolve this issue.

The probe used in making stagnation pressure measurements in the arcjet plume (cf. Figure 14) consists of a 10-cm-long by 1.3-cm-diam. (o.d.) aluminum tube, with a 10 degree lip, attached to an MKS model 627 Baratron capacitance manometer which was calibrated to a pressure of 0.013 Pa (1×10^{-4} Torr). The purpose of the chamfer is to minimized edge effects at the collection orifice by ensuring that most incident particles are directed to the pressure measuring volume of the sensor[22]. Recent analytical and particle-in-cell (PIC) code modeling at PEPL suggest that the error in this measurement device, *at these conditions,* is approximately ±30%.

Output from the Baratron was processed with an MKS PDR-C-1C display and the LabVIEW data acquisition system. The probe assembly was connected to a boom that was placed on the probe positioning system. Through use of the theta table, the probe could be rotated to more than ±90 degrees from the thruster axis.

Figure 15 shows typical data from a theta scan from -90 to 90 degree, with the probe at a fixed spatial location approximately 0.5 meters from the nozzle exit. The

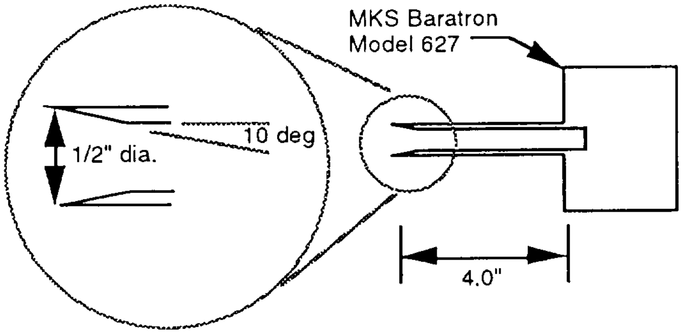

Figure 14: Detail of the impact pressure probe assembly showing 10 degree internal chamfer on probe lip.

local flow angle can be interpreted as the point corresponding to the maximum pressure reading (i.e., when the probe is pointed directly into the oncoming flow). The figure shows that the local flow angle at this spot is approximately 20 degrees with respect to the thruster axis. This process can be repeated at various axial and radial locations to map the local flow field in terms of direction. An example of this is shown in Figure 16 which shows flow angle as a function of radial position 48 cm downstream of nozzle exit. Flow angle at each spot is determined from recording the angle of maximum pressure when the probe is rotated through 180 degrees at a fixed spatial location. The curve on this figure shows flow angle as computed from the source flow model described below. As is expected, the flow angle of the expanding plume increases with radial position. Although few points are reported, the fact that the data corroborate the source flow code and are symmetric about the thruster centerline (0 inch position) is especially encouraging.

Although it has been demonstrated that this technique can be used to qualitatively map the far-field flow pattern, it was of particular interest to determine if absolute pressure measurements could be made. To this effect, the Revised Plume Model code (RPM) from the NASA Johnson Space Center (JSC) was used to generate dynamic pressure simulations for the arcjet. The code is capable of generating a complete spatial flow-field map of dynamic pressure values for a nozzle exhausting into vacuum. The input parameters for the code include nozzle geometry, stagnation pressure and temperature, molecular weight, γ, and the boundary layer thickness at the nozzle exit.

The RPM code was written at NASA JSC with the goal of obtaining an accu-

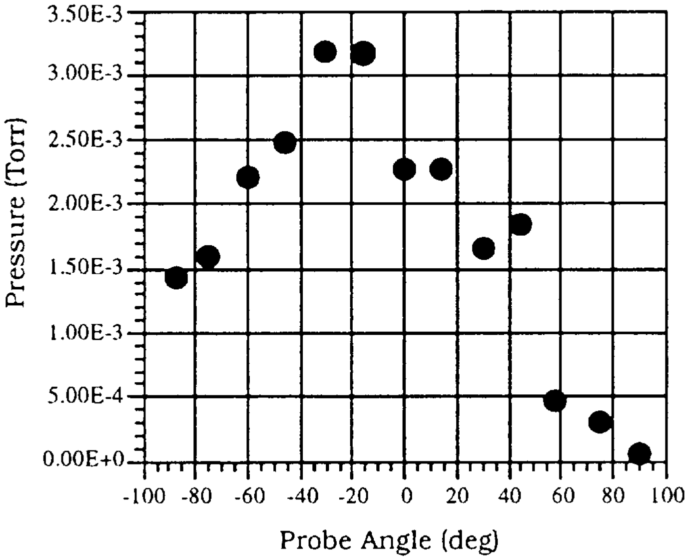

Figure 15: Impact probe pressure vs. probe angle for data taken 47.6 cm downstream of the exit plane and 25.4 cm radially from the plume center.

rate model of the Shuttle Orbiter's Primary Reaction Control System (PRCS) nozzle plumes[23]. The code has been ground verified and modified using conventional cold gas expansion nozzles in a large vacuum chamber. No attempt was made at modifying the code for arcjet plumes. The motivation behind the use of RPM in this research was to test the validity of this model in the mid to far-field region of a 1 kW arcjet plume and to use it for comparison against impact pressure probe data.

Since the ionization fraction of the plume is low ($< 10^{-2}$), a high temperature neutral gas with 30% dissociated hydrogen was assumed for the model. This level of dissociation was estimated by assuming the flow to be in chemical equilibrium in the constrictor and frozen throughout the nozzle. Thus, the very small amount of ionization in the plume combined with the simple nozzle geometry will create a plume flow field that is similar to that of a conventional rocket with a high exhaust temperature[24]. Successful extension of conventional plume flow field solvers such as RPM to the plume

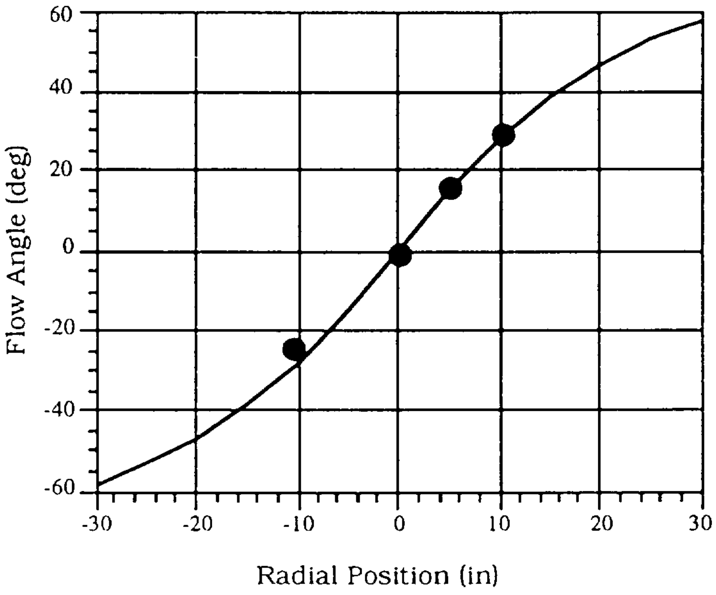

Figure 16: Flow angle, as determined from impact probe measurements, vs. radial position 25 cm downstream of the nozzle exit. Solid curve represents source flow model prediction

of arcjets provides a simple method of predicting the flow of the neutral species from these devices. This application, if successful, would eliminate the need for development of costly arcjet solvers employing complicated (and unnecessary) models to account for ionization and dissociation in the plume.

The RPM code is based on a source flow model in that the neutral gas species are assumed to behave as though they were emitted from a supersonic point source located at the nozzle exit plane. The density of this flow is assumed to fall off as the radius squared in the inviscid core of the plume to satisfy mass conservation. An exponential decay factor is applied to the gas originating from the nozzle boundary layer. The fundamental underlying equation of the model is given below for dynamic pressure, q,

$$q = A_o P_b \frac{A^*}{A_e} (\frac{r_e}{r})^2 \frac{\gamma}{\gamma - 1} (\frac{2}{\gamma + 1})^{\frac{1}{\gamma - 1}} \xi(\theta). \tag{11}$$

For $\theta < \theta_o$

$$\xi(\theta) = [\cos(\frac{\pi}{2} \frac{\theta}{\theta_{\mathrm{L}}})]^{\frac{2}{\gamma - 1}}. \tag{12}$$

For $\theta_o \leq \theta \leq \pi$,

$$\xi(\theta) = [\cos(\frac{\pi}{2} \frac{\theta}{\theta_{\mathrm{L}}})]^{\frac{2}{\gamma - 1}} \mathrm{e}^{-(\beta + 2\chi)(\theta - \theta_o)}. \tag{13}$$

The parameter θ_o is defined as the angle where the inviscid plume core meets the boundary layer gas in the nozzle, θ_{L} is the limiting Prandtl-Meyer expansion angle, and the parameters β and χ are related to the density and velocity decay in the nozzle boundary layer flow[24]. A_o and P_b are parameters related to the formation of the boundary layer and the supersonic expansion of the flow outside of the nozzle[25]. This model is expected to be most accurate within 60 degrees of the thruster axis.

Figure 17 shows comparisons between dynamic pressure profiles predicted by the code and impact pressure probe data at two axial locations (53 and 64 cm from the nozzle exit). As model inputs, the arcjet boundary layer thickness was estimated to be 1 mm at the exit, and the stagnation temperature and pressure were set at 3300°K and 0.27 MPa, respectively. Data points represent radial sweeps at discrete probe angles across the entire radial table (60 inches long) within a 50 degree cone from the nozzle. As the figure shows, at each axial location the envelope of data is enclosed in the profile predicted by the model. The model predicts higher pressures near the ends of the table (±30 in) than are measured. For these measurements, tank pressure was recorded at 0.019 Pa (1.4×10^{-4} Torr) with the side-mounted ionization gauges. Thus, the fact that dynamic and static pressure at the edge of the measurement region fall below the lower limit detectable by the Baratron (0.01 Pa) not only corroborates ionization gauge data, but suggests that the bulk of the neutrals flows within 2 meters of the plume center at these axial locations. Lastly, by comparing measured pressures with measured electron temperatures and number densities at these axial positions, and by assuming a heavy particle translational temperature of 2000°K, an upper limit to the on-axis neutral gas density was calculated to be $\sim 10^{13}$ cm^{-3}, corresponding to an ionization fraction of $\sim 10^{-4}$.

2.3 Results with the Stationary-Plasma Thruster

Under this grant, Dr. Sergey Khartov of the Moscow Aviation Institute (MAI), a world-renowned expert on the Stationary-Plasma Thruster (SPT), participated in electric

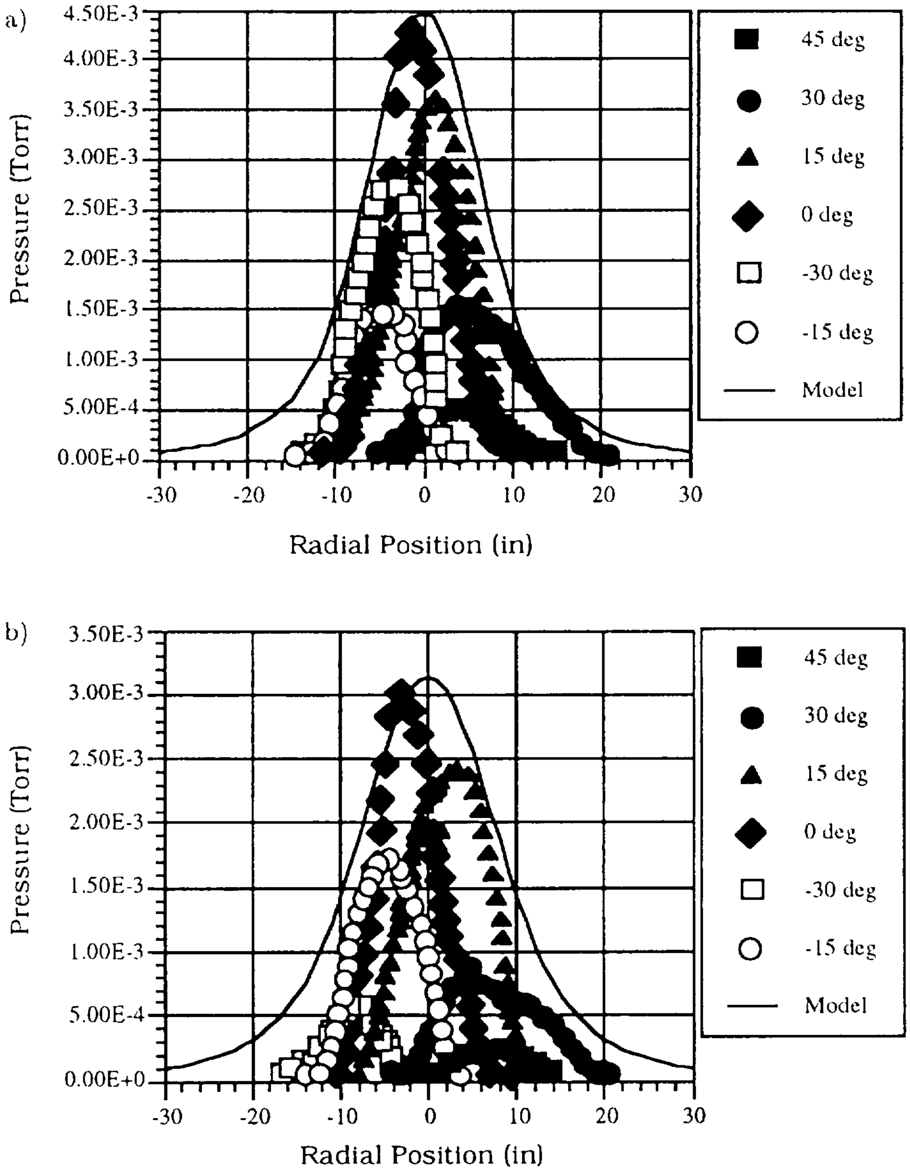

Figure 17: Impact pressure probe data at various angles vs. radial position at axial positions 53 [a)] and 64 cm [b)] from the nozzle exit.

propulsion research at the University of Michigan for five weeks as a visiting research scientist. Dr. Khartov brought a lab-model SPT that is roughly equivalent to the FAKEL-built SPT-100, three lanthanum hexaboride cathode inserts, and a 2.5-cm-diam. three-grid retarding potential analyzer (RPA). As part of an ongoing agreement between PEPL and MAI, these items were allowed to remain at PEPL for two years.

The thruster was operated at power levels between 400 W and 1.2 kW. Data included in this report (see figures below) were obtained at a nominal operating regime of 240 V, 3.4 A, and at a krypton propellant mass flow rate of 3 mg/s (10% cathode split).

The technique used to determine the plasma potential employed a variation of the traditionally used emissive probe scheme[26]. The tungsten spiral probe was run in two regimes to obtain data which were then used to determine the plasma potential. The cathode-emissive probe potential was ramped from zero to the near-plateau region of the curve. The first data sweep determined the current-voltage characteristics from the cold probe. The second sweep required probe heating while the near cathode region was kept at a constant floating potential by regulating the cathode heater. The point of intersection of the two I-V curves determined the plasma potential. This technique differs from that of using the derivative of the hot probe voltage-current characteristic and using the maximum of this curve (point of inflection) to determine plasma potential. In the future, both techniques will be compared.

For this test, the emissive probe was attached to the front face of the SPT at the 2 o'clock position (cathode was at the 12 o'clock spot). Figure 18 displays one set of emissive probe data taken at this location. The initial segment of the heated probe curve where the current between the cathode and the probe is decreasing is the probe heating period during which the current in the probe is increased to 6 A.

As the figure shows, a 33 V drop exits between the cathode and the exit plane of the engine, suggesting that most of the acceleration takes place inside the engine. This result is consistent in that the region of intense ion acceleration (i.e., electric field) is in the portion of the thruster where the electrons are most magnetized. The large insulator erosion that is associated with this device also supports this finding.

An RPA was used to determine the distribution of ion energies in the plasma. It was built at the MAI and features a 1-inch-diam. face and three stainless steel grids. The first grid floated to minimize perturbations to the plasma, the second grid repelled the electron current at -30 V (with respect to the cathode), and the third grid was the ion retarding grid.

Figure 19 a) and b) contain data taken by the probe. As Figure 19 a) shows, very little current is collected beyond a retarding potential of 300 V and no negative current was observed at 400 V. The average potential drop that the ions are expected to experience at this thruster setting is approximately 200 V. Thus, the ion energy

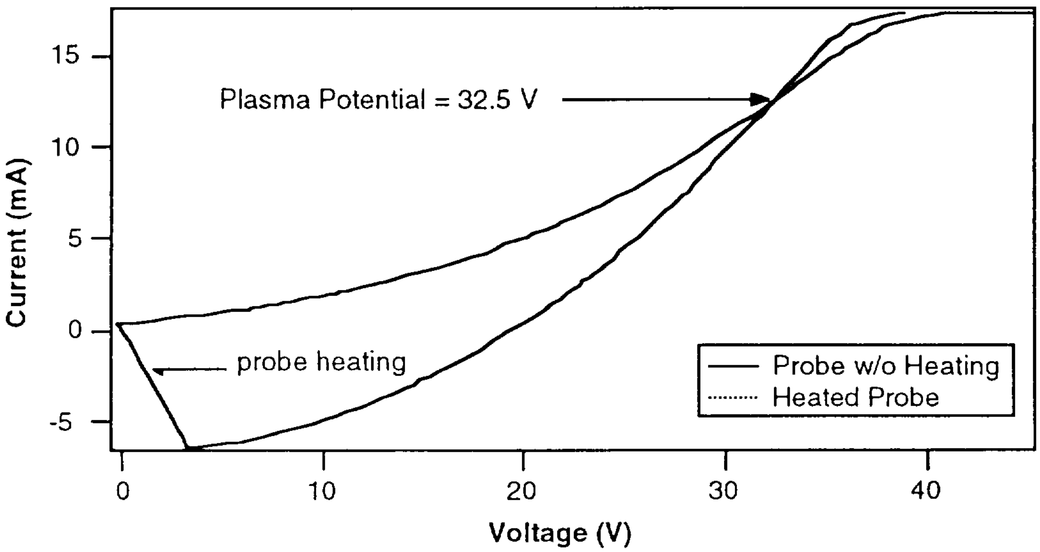

Figure 18: Current-voltage characteristics of the emissive probe with 4.1 V keeper potential and krypton propellant. Potential is measured with respect to the cathode.

distribution was expected to peak at ~200 V. However, as Figure 19 b) shows, the peak takes place at 180 V. This discrepancy may be an indication that the magnetic field topology of the lab-model device is not well tuned in comparison to the FAKEL-built engine, or that our RPA voltage is off-set by 10-20 V. Experiments will be conducted over the next year of support to determine the cause of this discrepancy.

References

[1] Patterson M.J., Robinson, T.D., Schemmel, T.D., and Burgess, D.R., "Experimental Investigation of a Closed-Drift Thruster," AIAA-85-2060, 18th *International Electric Propulsion Conference*, Alexandria, Virginia, September 30–October 2, 1985.

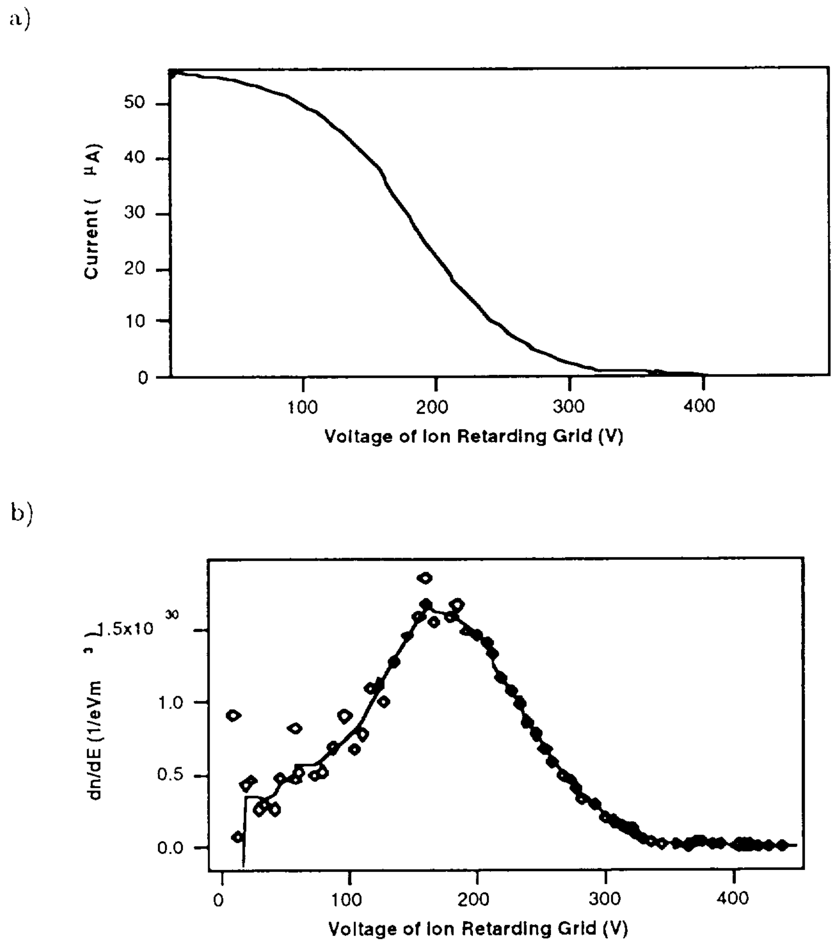

Figure 19: RPA current-voltage characteristics and ion energy distribution 0.5 m downstream of thruster exit plane along thruster axis.

[2] Jahn, R.G., Physics of Electric Propulsion, McGraw Hill Book Company, NY, 1968.

[3] Pivirotto, T., King, D., Deninger, W., and Brophy, J., "The Design and Operating Characteristics of a 30 kW Thermal Arcjet Engine for Space Propulsion," AIAA-86-1508, 22nd *Joint Propulsion Conference*, Huntsville, Alabama, June 16–18,1986.

[4] Carney, L.M., and Sankovic, J.M., "The Effects of Arcjet Thruster Operating Conditions and Constrictor Geometry on the Plasma Plume," AIAA-89-2723, (NASA TM-102285), presented at the 25th *Joint Propulsion Conference*, Monterey, California, July 10–12, 1989.

[5] Curran F.M., Bullock, S.R., Haag T.W., Sarmiento, C.J., and Sankovic J.M., "Medium Power Hydrogen Arcjet Performance," AIAA-91-2343, 27th *Joint Propulsion Conference*, Sacramento, California, June 24–27, 1991.

[6] Gallimore, A.D., Myers, R.M, Kelly A.J., and Jahn R.G., "Anode Power Deposition in an Applied-Field Segmented Anode MPD Thruster," AIAA-91-2343, 27th *Joint Propulsion Conference*, Sacramento, California, June 24–27, 1991.

[7] Sovey, J.S., and Mantenieks, M.M.,"Performance and Lifetime Assesment of Magnetoplasmadynamic Arc Thruster Technology," J.Propulsion, Vol. 7, No. 1 Jan–Feb, 1991, pp 71-83.

[8] Patterson, M.J., "Performance Characteristics of Ring-Cusp Thrusters with Xenon Propellant," AIAA-86-90, 22nd *Joint Propulsion Conference*, Huntsville, Alabama, July 16–18, 1986.

[9] Aston, G., Brophy, J., Garner, C., and Pless, L., "A Xenon Ion Propulsion Module for Enhanced Spacecraft Capability," AIAA-86-1393 22nd *Joint Propulsion Conference*, Huntsville, Alabama, July 16–18, 1986.

[10] Kaufman, H.R., "Technology of Closed-Drift Thrusters," AIAA-83-1398, 19th *Joint Propulsion Conference*, Seattle, Washington, June 27–29, 1983.

[11] Brown,C.O.,and Pinsley, E.A.,"Further Experimental Investigations of a Cesium Hall-Current Accelerator," AIAA Journal, Vol. 3, No. 5, May, 1965, pp. 853-859.

[12] Chubb, D.L. and Seikel, G.R., "Basic Studies of a Low Density Hall Current Ion Accelerator," (NASA TN D-3250), Feb.,1966.

[13] Morozov, A.I., Shubin, A.P., and Elizarov, L.I., "Modern State and Future of Electric Propulsion Thrusters," presented at the *Anniversary Specialist Conference on Nuclear Power Engineering in Space*, Institute of Physics and Power Engineering, Obninsk, May 15–19, 1990.

[14] Burgrova, A.I., Yermakov, Y.A., Morozov, A.I., and Yakunin, S.A., "A New Stage of Stationary Plasma Engine (SPE) Development," presented at the *Anniversary Specialist Conference on Nuclear Power Engineering in Space*, Institute of Physics and Power Engineering, Obninsk, May 15–19, 1990.

[15] Kaufman, H.R., Robinson, R.S., Day, M.S., and Haag, T.W., "End-Hall Thrusters," AIAA-90-2595, 21^{st} *International Electric Propulsion Conference*, Orlando, FL, July 18–20, 1990.

[16] Komurasaki, K., and Arakawa, Y., "Hall Current Ion Thruster Performance," AIAA-90-2594, 21^{st} *International Electric Propulsion Conference*, Orlando, Florida, July 18–20, 1990.

[17] Sankovic, J., Hamley, J., and Haag, T., " Performance Evaluation of the Russian SPT-100 Thruster," IEPC-93-094, 23^{rd} *International Electric Propulsion Conference*, Seattle, WA, September 13–16, 1993.

[18] Garner, C.E., Polk, J.E., Goodfellow, K.D., and Brophy, J.R., "Performance Evaluation and Life Testing of the SPT-100," AIAA-IEPC-93-091, 23^{rd} *International Electric Propulsion Conference*, Seattle, WA, September 13–16, 1993.

[19] Myers, R.M. and Manzella, D.H., " Stationary Plasma Thruster Plume Characteristics," AIAA-IEPC-93-096, 23^{rd} *International Electric Propulsion Conference*, Seattle, WA, September 13–16, 1993.

[20] Liebeskind, J. G., Hanson, R. K., and Cappelli M. A., "Flow Diagnostics of an Arcjet Using Laser-Induced Fluorescence," AIAA-92-3243, 28^{th} *Joint Propulsion Conference*, Nashville, TN, July 6–8, 1992.

[21] Hoskins, W. A., "Measurement of Population and Temperature Profiles in an Arcjet Plume," AIAA-92-3240, 28^{th} *Joint Propulsion Conference*, Nashville, TN, July 6–8, 1992.

[22] Koppenwallner, G., "The Free Molecular Pressure Probe with Finite Length Slot Orifice," *Rarefied Gas Dynamics,* 14_{th} *Symposium*, 1984, pp. 415-422.

[23] Fitzgerald, S. M., Bouslog, S. A., and Hughes, J. R., "Model for Predicting Orbiter PRCS Plume Impingement Loads," NASA Document No. JSC-26507, Jan., 1994.

[24] Simons, G. A., "Effect of Nozzle Boundary Layers on Rocket Exhaust Plumes," AIAA Journal, Vol. 10, Nov., 1972, pp. 1534-1535.

[25] Bird, G. A., "Breakdown of Continuum Flow in Freejets and Rocket Plumes," Rarefied Gas Dynamics. Part II. Progress in Astronautics and Aeronautics, Vol. 74.

[26] Kozlov, O.V., Electric Probes in Plasma, M.Atomizdat 1969 pp.100-109, 179-197.